



Europäisches Patentamt
European Patent Office
Office européen des brevets



Publication number: **0 550 189 A1**

EUROPEAN PATENT APPLICATION

Application number: 92311378.1

Int. Cl.⁵: G02F 1/315, G02F 1/03,
G01D 15/14

Date of filing: 14.12.92

Priority: 31.12.91 US 816452

Date of publication of application:
07.07.93 Bulletin 93/27

Designated Contracting States:
DE FR GB

Applicant: XEROX CORPORATION
Xerox Square
Rochester New York 14644(US)

Inventor: Hecht, David L.
2001 Barbara Drive
Palo Alto, California 94303(US)

Representative: Hill, Cecilia Ann et al
Rank Xerox Patent Department, Albion
House, 55-59 New Oxford Street
London WC1A 1BS (GB)

Electrooptic TIR light modulator image bar having multiple electrodes per pixel.

Increasing the addressing capability of an optical image bar (40) having a particular pixel center-to-center spacing (pixel pitch) is accomplished by employing a plurality of N electrodes (115a,b; 117a,b; 118a,b; 120a,b) per pixel (112,113). Compared to an optical image bar with one electrode per pixel, this provides N times as many locations for the electric potential transition which establishes the center of the pixel. The provision of multiple electrodes per pixel interval can be used to implement interlacing.

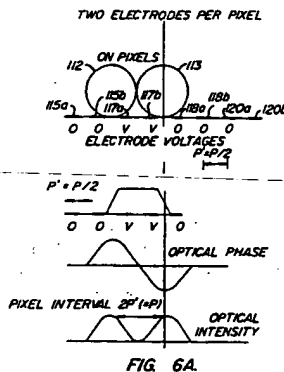


FIG. 6A.

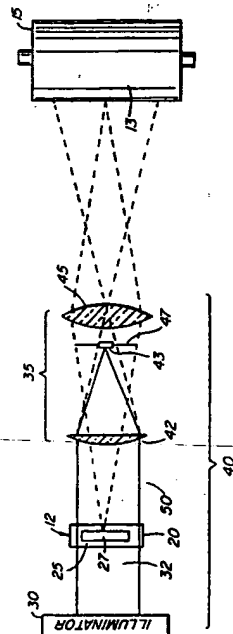


FIG. 2.

EP 0 550 189 A1

The present invention relates generally to optical image bar printing, and more particularly to an electrode array configuration for an image bar.

As a matter of definition, an "optical image bar" comprises an array of optical pixel generators for converting a spatial pattern, which usually is represented by the information content of electrical input signals, into a corresponding optical intensity profile. Although there are a variety of applications for such devices and a number of different fields, a significant portion of the effort and expense that have been devoted to their development has been directed toward their application to electrophotographic printing.

One type of image bar is based on the use of electro-optic (EO) total internal reflection (TIR) spatial light modulators, as described in U.S. Patent No. 4,396,252 to W.D. Turner. The modulator comprises a set of laterally separated, individually addressable electrodes, which are maintained closely adjacent a reflective surface of an optically transparent EO element, such as a lithium niobate crystal. In operation, substantially the full width of the EO element is illuminated by a transversely collimated light beam. This light beam is applied to the EO element at a near grazing angle of incidence with respect to its reflective surface, and is brought to a wedge-shaped focus on that surface so that it is totally internally reflected therefrom.

Voltages representing a linear pixel pattern are applied to the individually addressable electrodes, whereby localized fringe electric fields are coupled into the EO element. These fields produce localized variations in the refractive index of the EO element, so the wavefront of the light beam is spatially phase modulated in accordance with the pixel pattern as it passes through the EO element. The process is repeated for a sequence of pixel patterns, with the result that the wavefront of the light beam is spatially modulated as a function of time in accordance with successive ones of those patterns.

For image bar applications of such a modulator, schlieren optics are employed to convert the phase modulated wavefront of the light beam into a corresponding series of optical intensity profiles. If a printing function is being performed, these intensity profiles are in turn used to expose a photosensitive recording medium, such as a xerographic photo receptor, in accordance with the image defined by the successive pixel patterns.

U.S. Patent No. 4,940,314, issued July 10, 1990, to D.L. Hecht, addresses the problem that the effective diameter of the pixels produced by an EO image bar, as measured between their half power points at unity magnification, is approximately one-half the center-to-center spacing of its electrodes. Accordingly, such image bars not only

tend to cause image distortion because of spatial quantization errors, but also characteristically produce interpixel intensity nulls.

The '314 patent describes a technique wherein a discrete optical image bar sequentially generates a plurality of independent pixel patterns at different center wavelengths, and a prism system disperses those pixel patterns in accordance with their respective wavelengths to passively increase the spatial addressing capacity of the image bar. The wavelengths of the pixel patterns, the angular dispersion of the prism system, and the length of the optical arm along which the dispersion has effect are selected so that the pixel patterns are laterally offset from one another on the output image plane by a distance that is less than the center-to-center spacing of the pixels of any one of those patterns. As a general rule, the wavelength of the pixel patterns is cyclically or otherwise recurrently varied, so that the pixel patterns are interlaced in accordance with a predetermined lattice-like interlacing pattern.

It is an object of the present invention to enable the spatial addressing capability of a discrete image bar to be increased without resorting to mechanical motion or multiple-wavelength light sources.

In accordance with the present invention, an optical image bar having a particular pixel center-to-center spacing (pixel pitch) employs a plurality of N electrodes per pixel. Compared to an optical image bar with one electrode per pixel, this provides N times as many locations for the electric potential transition which establishes the center of the pixel.

The provision of multiple electrodes per pixel interval can be used to implement interlacing. This can be accomplished by uniformly spacing all pixel positions on one line by the pixel spacing, and then shifting all pixel positions on the succeeding lines by translating all pixel positions by one electrode interval.

The output image depends upon the input data voltage pattern on the electrodes and the spatial frequency response of the image bar. To the extent possible, it is desired that there be an ON pixel for each voltage step between adjacent electrodes, and that individual pixels be of substantially the same shape and size regardless of the data pattern. The invention is based in part on a recognition that the pixel size and quality resulting from a voltage difference between electrodes are determined primarily by the overall image bar spatial frequency response, which is not changed substantially by subdividing the electrodes. Accordingly, a set of preferred physical parameters can be determined by selecting parameter values to provide the desired spatial frequency response. This is made

possible by an improved understanding of the way that the physical parameters affect the frequency response.

It has been found that the parameter values that optimize the spatial frequency response do not necessarily optimize diffraction efficiency, and that other considerations might dictate non-optimum values. For example, it may be desired to use illumination conditions and electrode lengths that optimize efficiency, but do not optimize spatial frequency response. Under such conditions, it is sometimes possible to obtain the desired frequency response by using a compensation filter and thus simultaneously optimize efficiency and spatial frequency response. The filter may be chosen to define the spatial frequency response over the entire range of relevant frequencies, depending on the other parameters.

By way of example only, embodiments of the invention will be described with reference to the accompanying drawings, in which:

Fig. 1 is a schematic side view of the optical train of an optical image bar printer;

Fig. 2 is a schematic top view of the optical train of the printer;

Fig. 3 is a partly cut away bottom view of the EO modulator of the printer;

Fig. 4 is a simplified block diagram of the electronic control system of the printer;

Fig. 5A shows schematically a prior art electrode and pixel configuration, and plots of electrical potential, phase shift, and recorded pixel intensity;

Fig. 5B shows the minimum shift possible for the configuration of Fig. 5A;

Fig. 6A shows schematically an electrode and pixel configuration, and plots of electrical potential, phase shift, and recorded pixel intensity for a system in accordance with the present invention;

Fig. 6B shows the minimum shift possible for the configuration of Fig. 6A;

Figs. 7A-C show various interface patterns;

Figs. 8A-H show the amplitude and frequency response for differential encoding; and

Figs. 9A-H show the optimization of the image bar spatial frequency response by selection of an appropriate grazing angle, electrode length, and spatial filter.

by any convenient drive mechanism in the direction of the arrow 17. Nevertheless, other xerographic and non-xerographic recording media, including photoconductively coated belts and plates, as well as photosensitive films and coated papers could be used. Thus, in the generalized case, recording medium 13 should be visualized as being a photosensitive medium which is exposed while advancing in a cross-line or line pitch direction relative to modulator 12.

Fig. 3 is a partially cut-away bottom view of EO spatial light modulator 12. In keeping with standard practices, the modulator comprises an optically transparent EO element 20, such as an optically polished, y-cut crystal of lithium niobate, and a plurality of individually addressable electrodes 22. Electrodes 22 are deposited on, or held closely adjacent, a longitudinal reflective surface 25 of EO element 20. For example, they may be integrated with their addressing and drive electronics on a VLSI silicon circuit 27, and the modulator may then be assembled so that the electrodes are pressed against the reflective surface (by any convenient mechanism not shown). Typically, electrodes 22 extend lengthwise along EO element 20 and are transversely spaced on more or less uniformly displaced centers.

In operation, an illuminator 30 supplies a transversely collimated light beam 32 which is expanded by any convenient optical elements not shown) if and as required to illuminate substantially the full width of EO element 20. This light beam is brought to a wedge-shaped focus at a near grazing angle of incidence on the reflective surface of the EO element and is totally internally reflected therefrom. Successive sets of data samples are sequentially applied to electrodes 22, whereby the phase front of light beam 32 is spatially modulated while passing through EO element 20 in accordance with successive pixel patterns as a function of time.

The beam direction relative to the EO modulator is characterized by a grazing angle γ and a skew angle θ . The grazing angle is the angle between the center of the beam and the plane of the reflecting surface, measured outside the modulator. The skew angle is the projected angle of the beam relative to the direction of the electrodes. The drawings show axial operation (skew angle of zero).

A central dark field schlieren imaging subsystem 35 (Figs. 1 and 2) converts the phase modulated wavefront of light beam 32 into a corresponding intensity profile. The combination of modulator 12 with illuminator 30 and schlieren imaging subsystem 35 is an example of what is referred to herein as a discrete image bar 40.

A central dark field system suitably includes an objective lens 42 for focusing the transversely col-

System Overview

Figs. 1 and 2 are schematic side and top views illustrating the optical train of a line printer 10 having an EO spatial light modulator 12 for printing an image on a photosensitive recording medium 13. As shown, the recording medium is a photoconductively coated drum 15 which is rotated

limited zero order diffraction components of light beam 32 (collectively represented by solid line rays in Fig. 2) onto an opaque stop 43. The distance between EO element 20 and lens 42 is exaggerated. In a specific embodiment, the two are close so that lens 42 acts as a field lens. The zero-order components of light beam 25 are blocked because the stop is centrally located in the rear focal plane of the field lens, but the higher order diffraction components (collectively represented by broken line rays in Fig. 2, together with broken line cones for a single pixel) scatter around stop 43 and are collected by an imaging lens 45. Lens 45, in turn, focuses them on recording medium 13 with a predetermined magnification.

As will be described below, the imaging subsystem may include a compensating spatial filter 47 located in a far field plane, which may be the same plane as that of stop 43. Such a spatial filter would be used as one way to optimize the spatial frequency response of the image bar in order to produce uniform pixels of the desired size.

Fig. 4 is a block diagram illustrating circuitry for communicating data to electrodes 22 and controlling illuminator 30. Basic timing for the circuitry and the operations described below is established by a clock generator 58. An incoming data stream is input to a data buffer 65, encoded at a differential encoder 67, and communicated to address decoding circuitry 70. A controller 75 manages the data flow through the buffer and encoder, and provides sequential addresses to decoding circuitry 70 so as to cause a line of data to be applied to electrodes 22 during a data loading interval. Voltages corresponding to the data values are held on the electrodes during a subsequent data hold interval, and the illuminator is turned on and then off during the data hold interval to effect recording of the line of data. The process is then repeated for subsequent lines.

Multiple Electrodes Per Pixel

Figs. 5A and 5B illustrate the relationship of the pixels and electrodes in a typical prior art configuration. The top half of Fig. 5A shows a pair of adjacent pixels 102 and 103 resulting from a pattern of differentially encoded voltages on a set of electrodes 105, 107, 108, and 110. In this configuration, the pixels are characterized by a center-to-center spacing of P (pixel pitch), which also corresponds to the center-to-center spacing of the electrodes. Adjacent ON pixels are shown as touching circles, but it should be understood that the intensity distribution across a pixel is such that a typical pixel has a full width at half intensity of approximately $P/2$, so that the pixels are characterized by interpixel nulls.

The data is differentially encoded so that an ON pixel is produced at locations between electrodes that are at different voltages. The voltages on the electrodes in Fig. 5A are 0, V , 0, and 0, thus providing for an ON pixel centered between electrodes 105 and 107, and one between electrodes 107 and 108, as defined by the differential encoding of the signal on the electrodes. As described above, ON pixels will be produced resulting from the modulation caused by the differential voltage between electrodes 105 and 107 and between electrodes 107 and 108. Since there is no voltage differential between electrodes 108 and 110, no ON pixel is formed. Fig. 5A also shows the approximate electrical potential at the surface of EO element 20, the amplitude of the electro-optical phase shift produced by the resultant electric field, and the optical intensity resulting at the image plane of schlieren imaging system 35.

The minimum transverse shift of pixel locations is defined by the electrode spacing. As shown in Fig. 5B, when the voltage pattern is shifted to the right by one electrode interval, a corresponding shift in the pixel pattern occurs. Accordingly, when the desirability of shifting pixel patterns by less than a full pixel width was recognized, the prior art utilized mechanical or dispersive means to effect the desired displacement.

Figs. 6A and 6B show the electrode and pixel configuration, and the minimum shift possible when a multiple-electrode-per-pixel configuration according to the present invention is used. Fig. 6A shows a pair of ON pixels 112 and 113 resulting from a set of voltages on a set of electrode pairs 115a-b, 117a-b, 118a-b, and 120a-b. In this case, the electrodes have a center-to-center spacing of $P' = P/2$, but the voltage does not change any more frequently than once every two electrodes. Thus, the minimum ON pixel center-to-center spacing is $2P' (= P)$. Fig. 6A also shows the electrical potential, electro-optical phase shift amplitude, and optical intensity for this configuration.

Fig. 6B shows the resultant pixel pattern when the voltages are shifted one electrode to the right. In this case, the pixels maintain the same minimum pixel pitch P and size, but are shifted by a distance of $P' (= P/2)$.

At first glance, it would appear that it would be possible to pack the pixels more closely together by allowing the separation of transitions to be as close as the electrode pitch P' . However, the result could be excessive interference between adjacent ON pixels.

While the specific example of two electrodes per pixel interval is illustrated, the technique is readily extended to any plurality of N electrodes per pixel (i.e. electrode pitch P' equals $1/N$ times the minimum pixel pitch P). In such case, the

above mentioned constraint is that the encoding must result in groups of at least N electrodes at the same potential. However, there is no requirement that the groups of electrodes at the same potential be integral multiples of N . Thus, the enhanced addressability allows ON pixels at separations of other than integral multiples of NP , still subject to the constraint that the separation of transitions be at least NP .

Interlacing may be implemented by uniformly spacing all pixel positions on one line by the pixel spacing P , and then shifting all pixel positions on succeeding lines by translating all pixel positions by an electrode interval (P/N). The specific case illustrated above, namely $N = 2$, is of practical importance since it enables two-line interlace. The significance of this is that the typical pixel size is approximately $P/2$ in diameter so that the interlace allows filling of interpixel nulls. It is noted that this method does not inherently provide cross-scan image translation to compensate for recording medium motion between successive scan lines. Unless the medium is stopped for each scan line group, the result is a diamond interlace raster as shown in Fig. 7A. Directly recording rectangular raster data on the diamond lattice will result in systematic cross-scan displacement for alternate pixels along the interlaced lines. This may or may not be a serious effect, depending on image content, recording process, and visual effects. For example, modification to digitized font designs can be used to compensate for this. The diamond interlace raster can be advantageous if the recorded information is appropriately spatially sampled or interpolated, as for example in an electronic reprographics system where the read-in sample locations are inherently independent of image edge location.

Fig. 7B shows the result of interlace with cross-scan compensation.

Fig. 7C shows how the displacement effect can be made negligible by switching the modulator back and forth rapidly between the interlaced data sets. This could be implemented by rewriting the data lines, which requires increased modulator data input bandwidth, or by employing a VLSI driver chip with internal storage of the data of the two interlaced lines.

Preferred Physical Configuration

The output image depends upon the input data voltage pattern on the electrodes and the spatial frequency response of the overall optical system. This is determined by the intrinsic frequency response of the modulator itself, and the frequency response of other portions of the optical system, such as the spatial filter (if present). To the extent possible, it is desired that there be an ON pixel for

each voltage step between adjacent electrodes, and that individual pixels be of substantially the same shape and size regardless of the data pattern.

The intrinsic spatial frequency response of the modulator depends on the physical properties of the modulator, including the electrical and optical properties of the material and the electrode geometry (length and pitch). The overall frequency response also depends on the illumination conditions and the spatial filter. As will be discussed below it is possible to select a physical configuration that suppresses crosstalk and provides high efficiency and uniform pixel size and shape.

It is convenient to define normalized grazing and skew angles G_0 and S_0 , in units of the inter-order angle (the separation of the 0th and 1st diffraction orders), and to define normalized spatial frequency F , drive voltage V_T , and electrode length Q_0 as follows:

$$G_0 = \gamma / (\lambda / (n\lambda_0))$$

$$S_0 = \theta / (\lambda / (n\lambda_0))$$

$$F = f\lambda_0$$

$$Q_0 = 2\pi L\lambda / (n\lambda_0^2)$$

$$V_T = 2\pi n^2 r \lambda_0 V(f) / \lambda^2$$

where

γ = grazing angle (the angle between the beam and the surface of the electro-optic element)

θ = skew angle (the angle between the beam and the direction of the electrodes)

f = spatial frequency

$V(f)$ = peak-to-peak voltage of the TIR surface potential spectrum component at spatial frequency f

L = electrode length

λ = optical wavelength

n = optical index of refraction

λ_0 = EO spatial modulation period (2N times electrode pitch, or 2 times minimum pixel pitch P)

The diffraction efficiency η as a function of spatial frequency for planewave illumination can be approximated by combining the physical optics diffraction theory results for long electrode length, which gives proper results at high spatial frequencies, with a geometrical optics diffraction analysis for finite electrode length, which is valid for the low spatial frequencies where total internal reflection diffraction suppression effects are small. The resulting expression for η is as follows:

$$\eta = H_Q^2 V_T^2 E G_0^2 \operatorname{Re} \{ (G_0^2 - 2FS_0 - F^2)^{1/2} \} / D$$

where

E = ratio of normal to tangential dielectric tensor components

$$D = \{[(1-E)F + 25_0 E]^2 + 4EG_0^2\}^2$$

$$H_0 = 1 - \exp[-|F|G_0 Q_0/(2E^{1/2})]$$

The quantity V_T is a function of spatial frequency, being a normalized version of $V(f)$ which is the peak-to-peak voltage of the TIR surface potential component at spatial frequency f . The quantity depends on the data encoded on the electrodes since the data defines the spatial frequencies that are present. For all pixels ON, the voltage alternates from electrode to electrode so the spatial period is twice the pixel pitch, the spatial frequency is the inverse of this, and the normalized frequency $F = 1$. In this case the value of V is approximately equal to the impressed voltage, differing by a geometrical factor near unity that depends on the electrode width relative to the gap between electrodes.

It should be noted that the equation gives the first order diffraction theory, which is valid for diffraction efficiencies up to about 30%. Beyond 30%, non-linear multiple scattering effects may become important and the linear system frequency response analysis may not be sufficient. The amplitude of the frequency response is given by $H(F) = \pi^{1/2} \text{sgn}(F)/V_T$.

Where differential encoding is used, it is desired that the diffracted light optical amplitude at a point is proportional to the difference in electrical potential between points spaced by the pixel pitch (which for the case of N electrodes per pixel is N times the electrode pitch). This calls for a response similar to the linear operator known as the finite difference operator.

Figs. 8A-B show an ideal step input and the finite difference response to the step input taken over an interval P , where P is the pixel pitch. Figs. 8C-D are corresponding views for a non-ideal step input. The finite difference operator (P) can be expressed as an odd impulse pair, namely $(P) = \delta(x + P/2) - \delta(x - P/2)$, as shown in Fig. 8E.

The frequency response is given by the Fourier transform of the finite difference operator. Fig. 8F shows the optimum frequency response for operation with differential encoding. The response varies as $\sin(\pi F/2)$, where $F = 1$ ($f = 1/(2P)$) corresponds to the fundamental "all pixels ON" diffraction component. Fig. 8G shows an acceptable response, which tracks the ideal response over the spatial frequency range $-2 \leq F \leq 2$ where $F = 2$ ($f = 1/P$) is the first zero of the desired frequency response. For one electrode per pixel encoding, or for the more general case where all the normalization is in terms of $2N$ times the electrode pitch (i.e., 2 times the pixel pitch) response at

higher frequencies is not required, as these components only contribute to pixel profile edge sharpness.

Fig. 8H shows the frequency response in the limit of long electrodes and large grazing angle. The response is substantially different from the frequency dependence that is desired. It is, however, possible to tailor the physical parameters to provide the desired frequency response.

In the long electrode limit, it can be shown that the efficiency at $F = 1$ is maximized at a relatively small grazing angle. However, for small grazing angles, the quantity $(G_0^2 - 2FS_0 - F^2)$ becomes negative for some higher but finite spatial frequencies, and therefore the response cuts off above a finite spatial frequency. Fortunately, this cutoff can be exploited to bring the spatial frequency response of Fig. 8H more in line with that of Fig. 8G.

For axial illumination ($S_0 = 0$), cutoff occurs when

$G_0 \geq F$, i.e., when the inter-order diffraction angle for a given spatial frequency equals or exceeds the input grazing angle. Axial illumination is of particular interest since the response is antisymmetric with respect to F as desired for differential encoding. Using G_0 substantially less than 2 would truncate part of the desired frequency response for differential encoding below $F = 2$. On the other hand, using G_0 substantially greater than 2 would reduce the diffraction efficiency and would make the frequency response depart from the desired form below $F = 2$ with a cutoff at $F = 2$. Therefore, $G_0 = 2$ and $S_0 = 0$ is a preferred illumination condition for the differentially encoded modulator. Fig. 9A shows the spatial frequency response for $G_0 = 2$ and $S = 0$, with a long electrode.

It is important to note that additional conditions are required to achieve the desired frequency response form in the frequency range $-1 \leq F \leq 1$. Two approaches to correcting this frequency response are selecting an optimum electrode length and providing a specially configured optical spatial frequency response filter.

If the electrode length is relatively short, the dependence of the factor H_0^2 in the efficiency equation becomes apparent. In fact, H_0 is approximately linear as a function of F , which means that it also approximates a sinusoidal function of F for small values of F . Fig. 9B shows the frequency response for a finite electrode length; this is clearly closer to the desired response. By selecting the appropriate electrode length, it is possible to fit the frequency response to the desired response in a low frequency region. More particularly, for $F \ll 1$, $H_0 = \sin(FG_0 Q_0/(2E^{1/2}))$, which will equal $\sin(\pi F/2)$ for $Q_0 = \pi E^{1/2}/G_0$. This provides the optimum frequency response, as shown in Fig. 9C. In terms of the physical variables this gives $L = E^{1/2} \lambda_0/(2\gamma)$

$$= E^{1/2} P / \gamma.$$

This optimum length is independent of the optical wavelength, so that in multi-wavelength operation, frequency response can be simultaneously optimized over a broad range of wavelengths. This is because the interaction path truncation is a geometrical optics effect independent of wavelength. For operation in lithium niobate with the tangential direction along the z crystal axis and the normal direction along the y crystal axis, $E = 1.54$ if clamped dielectric constants are effective (2.54 if unclamped dielectric constants are effective). For $E = 1.54$, and $G_0 = 2$, then the optimum value is $Q_0 = 1.95$. In this case, $H_0 = 0.792$ at $F = 1$ so that the efficiency for the "all pixels ON" condition for a given voltage is decreased by a factor $H_0^2 = 0.63$ compared to a very long electrode. Alternately, the compensating voltage increase is $1/H_0 = 1.26$. (For $E = 2.54$ and $G_0 = 2$, then $Q_0 = 2.50$ and the other quantities scale accordingly). In general, the clamped dielectric constants apply to electrodes switched at high frequency above acoustic resonance; unclamped constants apply below acoustic resonance.

Thus, the dependence of the diffraction efficiency on electrode length allows the selection of an electrode length that provides the desired spatial frequency response. However, the electrode length that optimizes pixel crosstalk suppression is not necessarily the electrode length that is desirable from other points of view. As noted above, the optimum electrode length results in a decrease in efficiency and an increase in the drive voltage required. Moreover, short electrodes may be difficult to align properly, thereby militating toward longer electrodes.

The discussion above is generally in terms of normalized variables, and the statements regarding optimum length assume a fixed minimum pixel pitch P . However, it is possible to have physically long electrodes that optimize both efficiency and frequency response if it is permissible to increase the pitch P (i.e. have the electrodes more widely spaced) while maintaining the normalized parameters the same.

To the extent that it is desired to use longer electrodes than are necessary to optimize the low spatial frequency response of the modulator, it is possible to use a spatial filter (a compensation filter) that provides the desired system response with long electrodes. Assuming the illumination conditions are chosen to result in a cutoff in the modulator's response (as shown in Fig. 9A), the spatial filter should have a transmission characteristic that approximates $|\sin(\pi F/2)|$ in amplitude and $\sin^2(\pi F/2)$ in intensity for absolute values of F less than about 1. This can be expressed in terms of the actual physical spatial dimension in the spatial

frequency plane, x , by the scaling relationship $x = Zf\lambda/(2P)$ where Zf is the focal length of objective lens 42. Figs. 9D and 9E show the amplitude and intensity profiles for a compensation filter that could be used to provide the desired frequency response. This corresponds to a pure absorption filter, and is readily realizable and applicable by such means as a variable density photographic emulsion.

Independent of these considerations, a stop is required to adequately attenuate the zero-order beam for sufficiently high contrast schlieren imaging. If the zero-order light is sufficiently collimated, the compensation filter can perform the function of this stop since in the region $-0.1 \leq F \leq 0.1$, the sine filter transmission is small (less than 1%). However, if the zero-order beam is not narrowly localized over the entire image field due to optical system aberration, an additional high absorption stop may be employed. It need not be tapered because of the simultaneous presence of the compensation filter.

If for some reason it is necessary to use non-optimum grazing angle and electrode length, it is still possible to obtain the desired frequency response solely by use of a compensation spatial filter. For example, in the long-electrode, high-angle case, the filter should have a transmission characteristic that is proportional to $|\sin(F/2)|$ in amplitude and $\sin^2(F/2)$ in intensity for $|F| < 2$. Figs. 9F and 9G show the filter characteristics. This filter requires no absorption at the fundamental frequency ($F = 1$) of the modulator (all pixels on response); the absorption reduces excess light and ringing in modulated pattern pixels only. Fig. 9H is a simplified schematic view, which also shows blocking the light above $|F| = 2$. It also shows the response relative to the physical device.

Conclusion

In summary, it can be seen that a technique has been described for increasing the spatial addressing capability of EO spatial light modulators. This is accomplished by modifying the design to one containing N electrodes per pixel. However, the conditions that tend to optimize the operation in the case of one electrode per pixel configuration apply equally well in the case of multiple electrodes.

While a number of embodiments are described above, various modifications, alternatives, and equivalents may be used. For example, a central bright field system (not shown) could be used to perform the conversion process, although it will be understood that such a change would reverse the logical relationship of the individual pixels within the intensity profile to the localized phase modula-

tion of the wavefront of light beam 32 (i.e., "bright" pixels would become "dark" pixels, and vice-versa, unless steps were taken to account for the reversal in the logical relationship). In such a case, however, the specific techniques for optimizing the spatial frequency response of the image bar might be different.

cause the frequency response to cut off at absolute values of f above about $1/P$, whereupon the spatial frequency response approximates $\sin(\pi Pf)$ for absolute values of f less than about $1/P$, where f is the spatial frequency.

Claims

1. A electrooptic light modulator system, comprising an electrooptic total internal reflection light modulator (12) having a set of electrodes (22), an electronic control subsystem for differentially encoding pixel data on the electrodes by applying corresponding voltages thereto in a manner that defines a minimum pixel pitch P , an illumination subsystem (30) for providing an input beam (32) to the modulator, which input beam is converted to a phase front modulated beam by the modulator and the voltages applied thereto, and an imaging subsystem (35) for converting the phase front modulated beam to an imaged beam having an intensity modulated profile corresponding to the pixel data, wherein:
 - the set of electrodes includes a plurality of N individually addressable electrodes (115a,b; 117a,b; 118a,b; 120a,b) for each pixel (112,113), with all electrodes in the set being at a center-to-center spacing of P/N ; and
 - the system is configured such that the drive voltage provided by the electronic control subsystem and the resultant pixel size are substantially the same as if the set of electrodes consisted of a single electrode per pixel with an electrode center-to-center spacing of P .
2. A system as claimed in claim 1 wherein the diffraction efficiency of the system is in part defined by a set of properties of the modulator and the illumination and imaging subsystems and is characterized by a spatial frequency response that approximates $\sin(\pi Pf)$ for absolute values of f less than about $1/P$, where f is the spatial frequency.
3. A system as claimed in claim 2, wherein the electrodes are characterized by a length chosen to cause the frequency response to approximate $\sin(\pi Pf)$ for small absolute values of f .
4. A system as claimed in any one of the preceding claims, wherein the input beam impinges on the modulator in a direction parallel to the electrodes and at a grazing angle chosen to

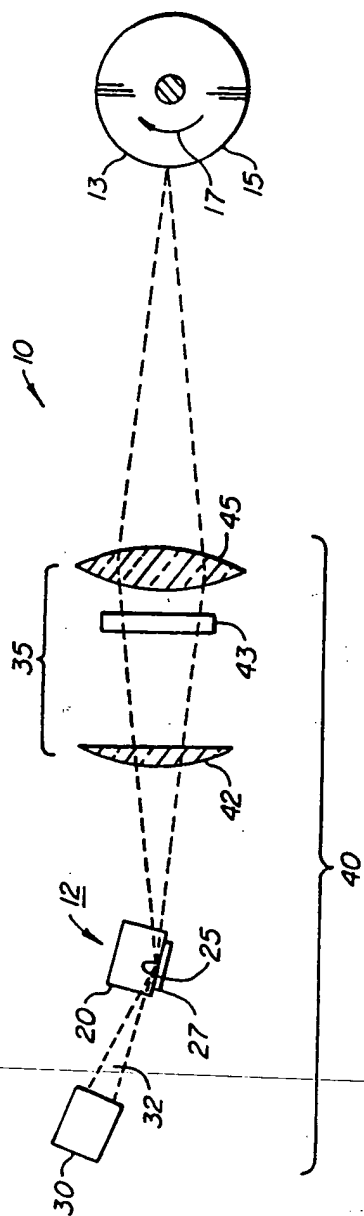


FIG. 1.

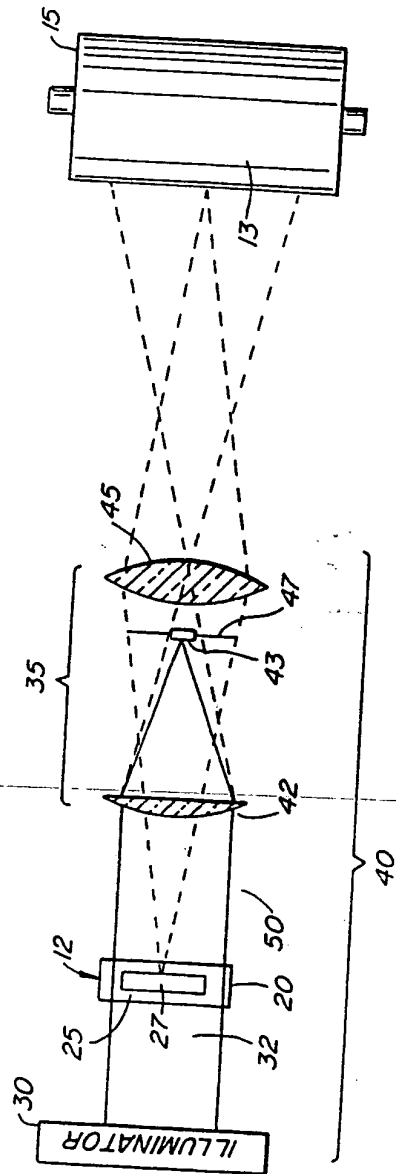
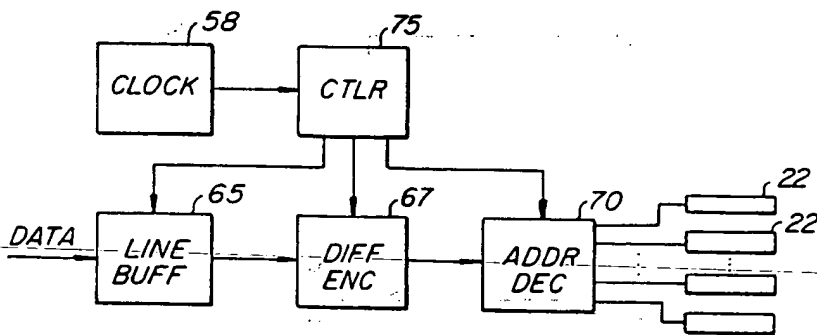
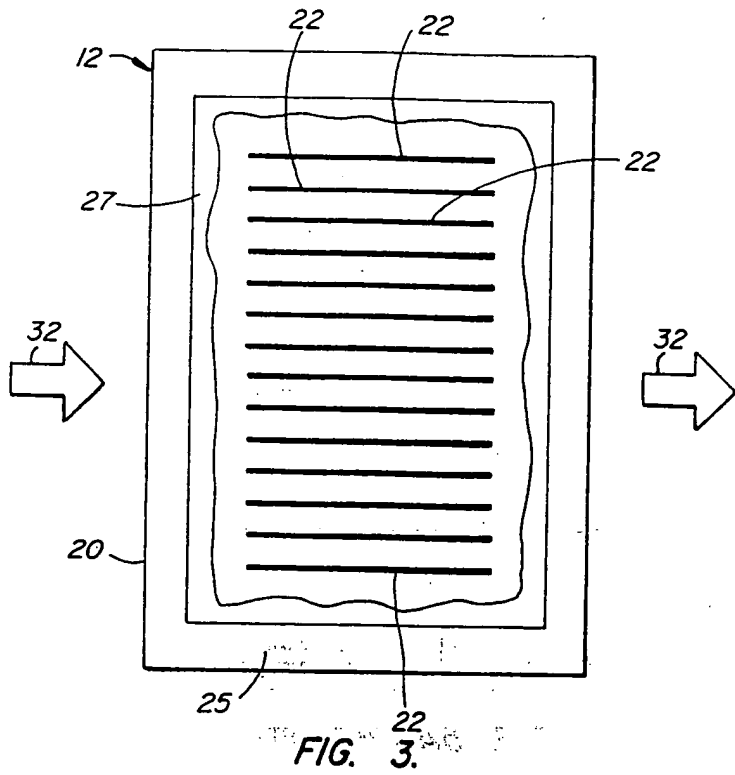


FIG. 2.



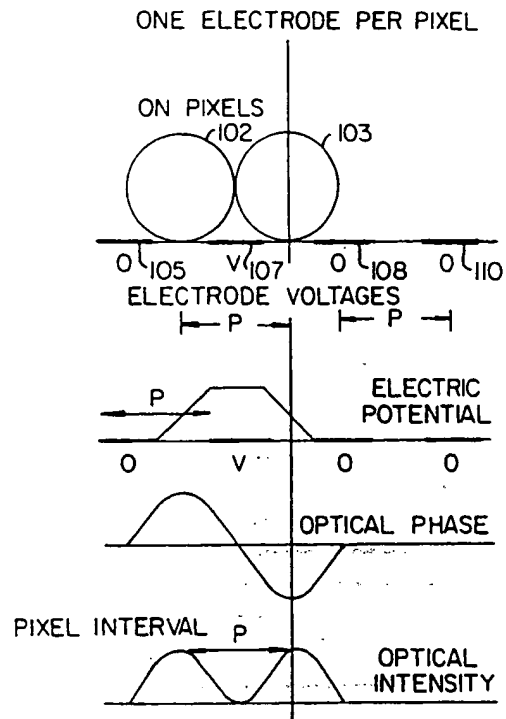


FIG. 5A. (PRIOR ART)

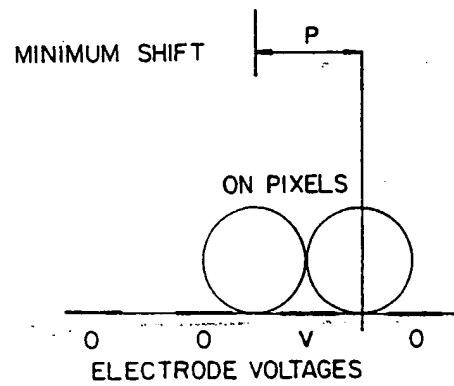


FIG. 5B. (PRIOR ART)

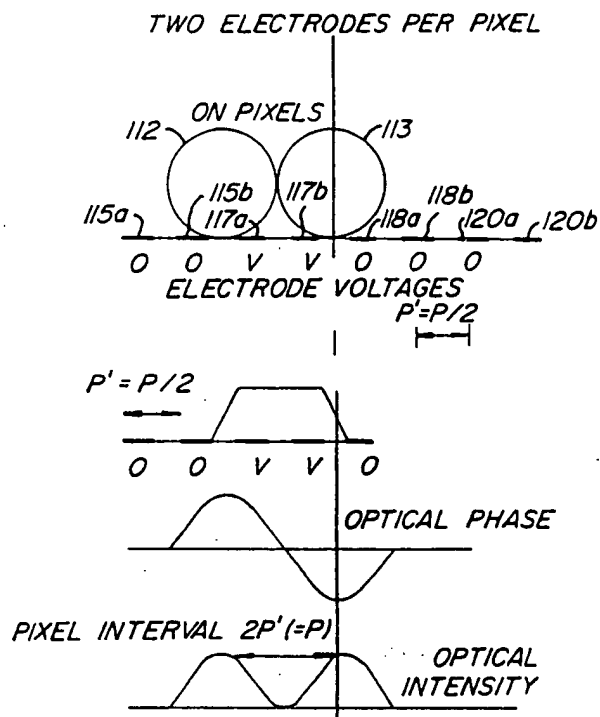


FIG. 6A.

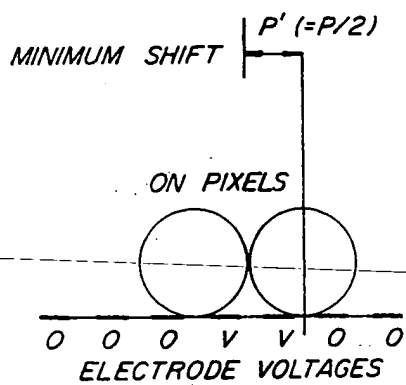
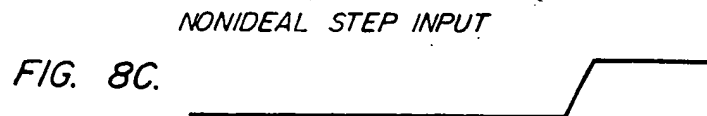
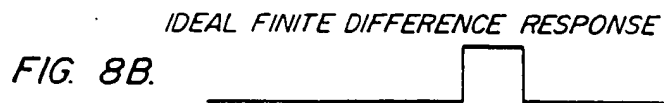
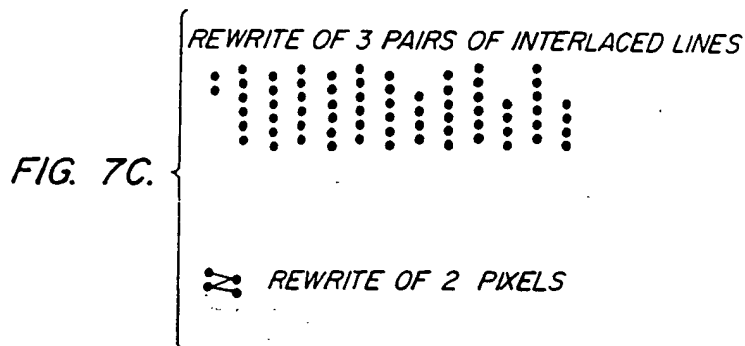
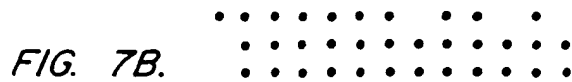
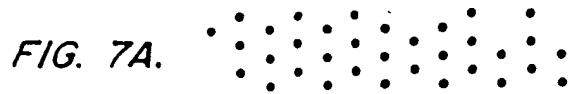


FIG. 6B.



FINITE DIFFERENCE
RESPONSE

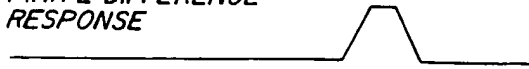


FIG. 8D.

DIFFERENTIAL ENCODING
IDEAL IMPULSE RESPONSE

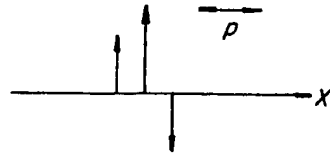


FIG. 8E.

DIFFERENTIAL ENCODING
IDEAL FREQUENCY RESPONSE

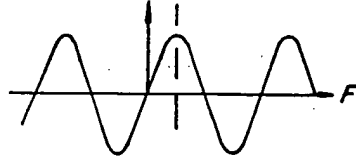


FIG. 8F.

SATISFACTORY FREQUENCY RESPONSE

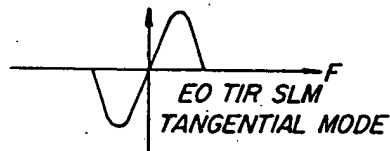


FIG. 8G.

LONG ELECTRODE
HIGH ANGLE FREQUENCY RESPONSE

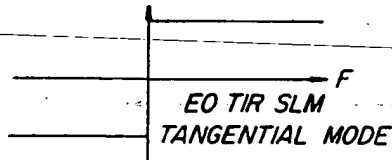


FIG. 8H.

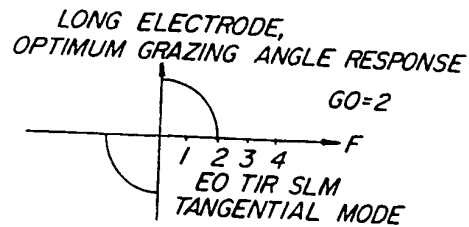


FIG. 9A.

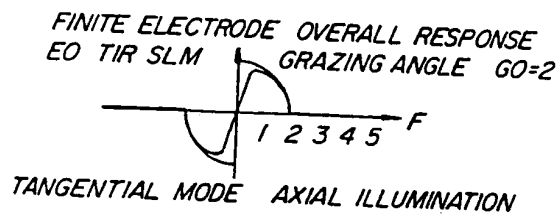


FIG. 9B.

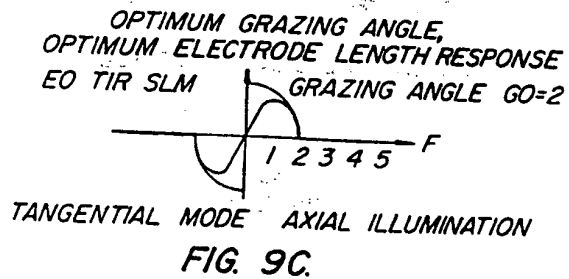


FIG. 9C.

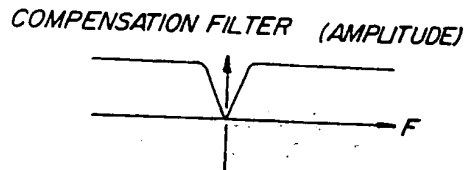
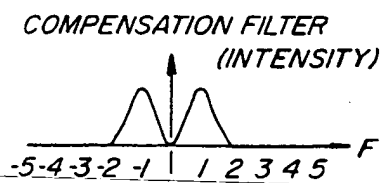
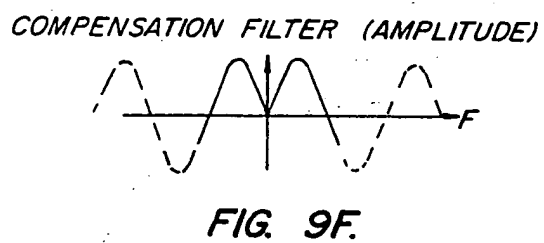
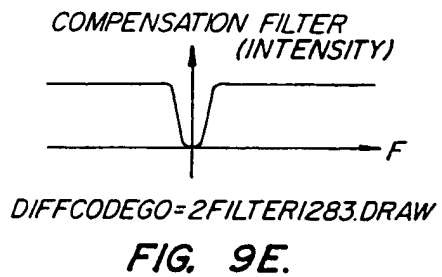


FIG. 9D.



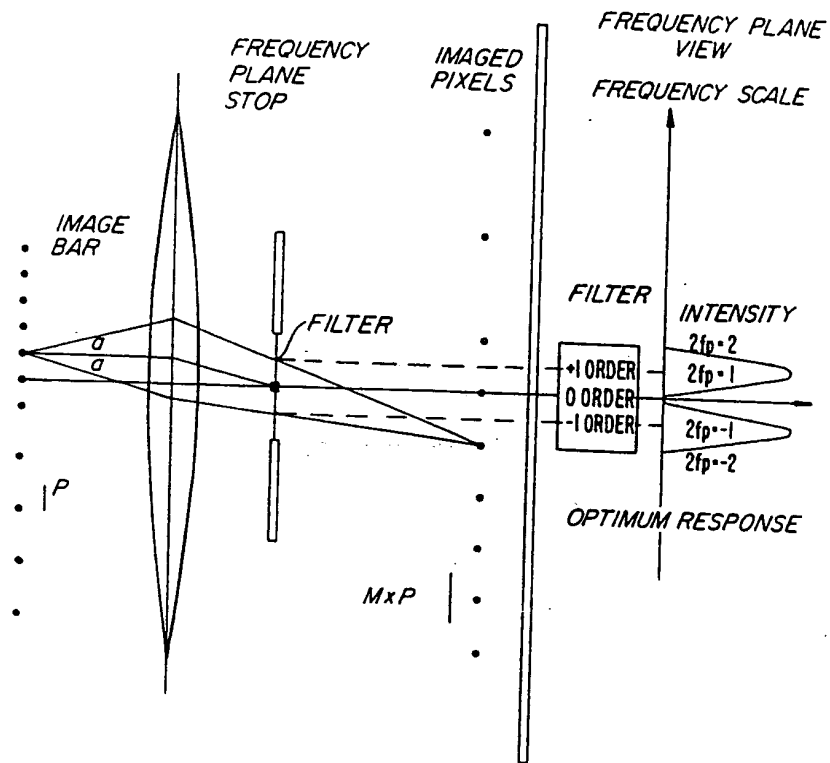


FIG. 9H.



European Patent
Office

EUROPEAN SEARCH REPORT

Application Number

DOCUMENTS CONSIDERED TO BE RELEVANT			EP 92311378.1
Category	Citation of document with indication, where appropriate, of relevant passages	Relevant to claim	CLASSIFICATION OF THE APPLICATION (Int. Cl.5)
A	<u>US - A - 4 780 732</u> (ABRAMOV) * Column 4, lines 5-68; column 6, lines 21-38 *	1	G 02 F 1/315 G 02 F 1/03 G 01 D 15/14
D, A	<u>US - A - 4 940 314</u> (HECHT) * Column 5, line 48 - column 7, line 12 *	1	
A	<u>EP - A - 0 229 506</u> (XEROX) * Column 3, line 53 - column 4, line 19; column 5, lines 26-46; column 6, line 9 - column 9, line 11 *	1	
A	<u>US - A - 4 750 815</u> (KATAOKA et al.) * Column 1, lines 11-55; column 2, line 56 - column 4, line 60; column 5, lines 8-13; fig. 10, 11 *	1	
D, A	<u>US - A - 4 396 252</u> (TURNER) * Abstract; fig. 4-8; column 4, lines 62-64 *	1	
The present search report has been drawn up for all claims			
Place of search VIENNA		Date of completion of the search 24-03-1993	Examiner GRONAU
CATEGORY OF CITED DOCUMENTS X : particularly relevant if taken alone Y : particularly relevant if combined with another document of the same category A : technological background O : non-written disclosure P : intermediate document T : theory or principle underlying the invention E : earlier patent document, but published on, or after the filing date D : document cited in the application L : document cited for other reasons A : member of the same patent family, corresponding document			

THIS PAGE BLANK (USPTO)